

2D MoS₂/Cu₂O on 3D mesoporous silica as visible-NIR nanophotocatalysts for environmental and biomedical applications

Gubakhanim Shahnazarova,^{a,b} Jessica C. Ramirez,^{a,b} Nour Al Hoda Al Bast,^{a,b} Jordi Fraxedas,^a Aritz Lafuente,^{a,b} Cristina Vaca,^{b,c} Marianna Sledzinska,^a Valentin Novikov,^{d,e} Carme Nogues,^b Josep Nogues,^{a,f} Albert Serra^{e,g}, Borja Sepulveda,^{*c} Maria J. Esplandiu^{*a}

- a. Dr. Gubakhanim Shahnazarova, Dr. Nour Al Hoda Al Bast, Jessica C. Ramirez, Aritz Lafuente, Dr. Marianna Sledzinska, Prof. Josep Nogues, Dr. J. Fraxedas, Dr. Maria J. Esplandiu
Catalan Institute of Nanoscience and Nanotechnology (ICN2), CSIC and BIST, Campus UAB, Bellaterra, E-08193 Barcelona.
- b. Dr. Gubakhanim Shahnazarova, Dr. Nour Al Hoda Al Bast, Jessica C. Ramirez, Aritz Lafuente, Cristina Vaca, Prof. Carme Nogues
Universitat Autònoma de Barcelona, 08193 Cerdanyola del Vallès, Barcelona, Spain.
- c. Cristina Vaca, Dr. Borja Sepulveda,
Instituto de Microelectrónica de Barcelona (IMB-CNM, CSIC); Barcelona, 08193, Spain
- d. Dr. Valentin Novikov,
Departament de Química Inorgànica i Orgànica, Secció Química Inorgànica, Universitat de Barcelona, Martí i Franquès, 1, E-08028, Barcelona, Catalonia, Spain
- e. Dr. Valentin Novikov, Dr. Albert Serra,
Institute of Nanoscience and Nanotechnology (IN2UB), Universitat de Barcelona, Barcelona, Catalonia, Spain.
- f. Prof. Josep Nogues, ICREA,
Pg. Lluís Companys 23, 08010 Barcelona, Spain
- g. Dr. Albert Serra,
Grup d'Electrodeposició de Capes Primes i Nanoestructures (GE-CPN), Departament de Ciència de Materials i Química Física, Universitat de Barcelona, Martí i Franquès, 1, E-08028, Barcelona, Catalonia, Spain.

Corresponding authors Email: borja.sepulveda@csic.es , mariajose.esplandiu@icn2.cat
Gubakhanim Shahnazarova and Jessica C. Ramirez contributed equally to this work

1. Electron energy loss spectroscopy (EELS) and energy dispersive X-ray spectroscopy (EDS) analysis

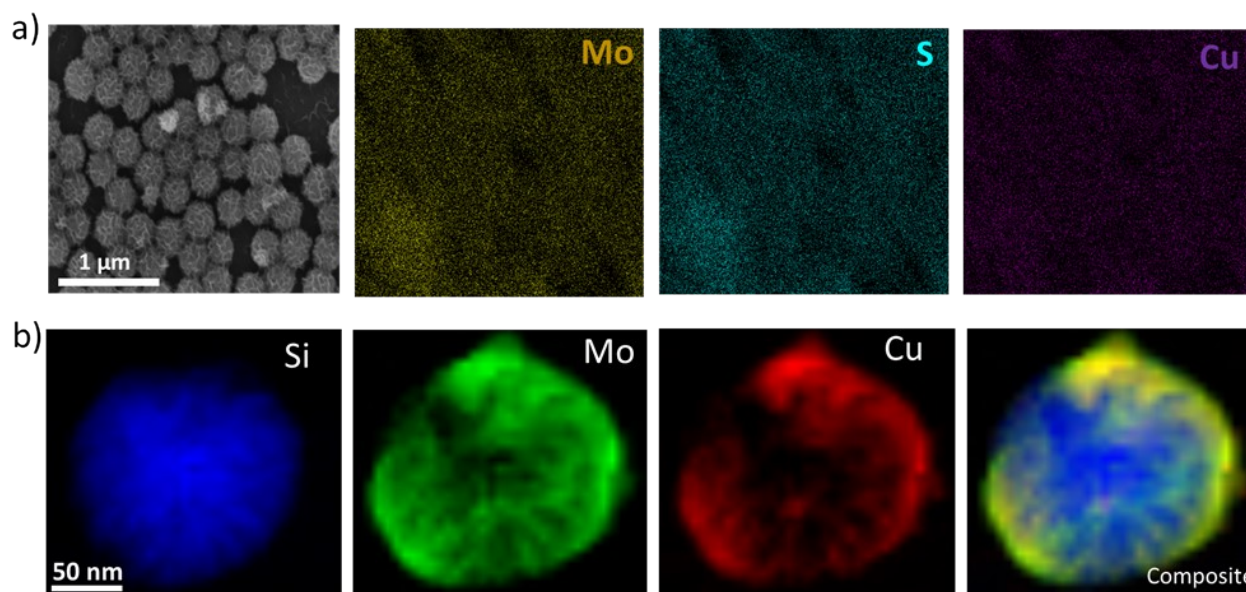


Figure S1. EDS (a) and STEM-EELS (b) mappings of the $\text{SiO}_2/\text{MoS}_2/\text{Cu}_2\text{O}$ samples.

2. X-ray Photoelectron Spectroscopy (XPS) analysis of Cu_2O

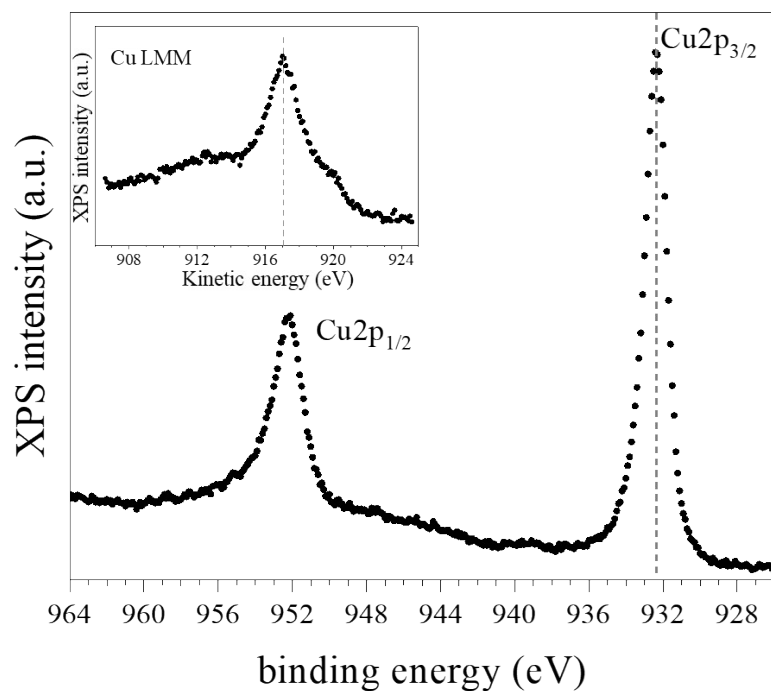


Figure S2. XPS spectra of the $\text{Cu}2\text{p}$ lines and the CuLMM Auger lines (inset) of the hydrothermal $\text{MoS}_2/\text{Cu}_2\text{O}$ nanoflakes.

3. Comparison of TC degradation with literature

Table S1. Comparison of reported studies on MoS₂-based photocatalysts for the degradation of tetracycline (TC) or its derivatives (OTC). k_N represents the normalized rate constant with respect to the catalyst dosage. TOC denotes the total organic carbon removal. Colored cells indicate the studies using low amount of catalyst. Note that the references in the last column correspond to those cited in the main text of the paper.

Photocatalyst	Light source	MoS ₂ preparation and precursors HT (hydrothermal) ST (solvothermal)	TC mg/L	Photocatalyst dosage	k (min ⁻¹) k _N (min ⁻¹ g ⁻¹)	% Degradation	TOC	Ref.*
C ₃ N ₄ /MoS ₂	Metal halide 250 W (λ > 420 nm)	HT, Sodium Molybdate, Thiourea	10	10 mg, (1g/L)	0.01294 min ⁻¹ , 1.294 min ⁻¹ g ⁻¹	90% (120 min)		63
n-ZnO/MoS ₂	Xe 300 W (λ > 420 nm)	HT, Sodium Molybdate, Thiourea	10	25 mg (0.5g/L)	0.0144 min ⁻¹ , 0.576 min ⁻¹ g ⁻¹	84% (120 min)		38
CuBi ₂ O ₄ /MoS ₂	Xe 300 W (λ > 420 nm), 89 mW/cm ²	Exfoliated MoS ₂ sheets	10	50 mg (0.5 g/L)	0.0095 min ⁻¹ , 0.19 min ⁻¹ g ⁻¹	76%, (120 min)	48%	64
MoS ₂ /Ag ₂ S/Ag		Hydrothermal Ammonium Molybdate, Thiourea	5	1 g/L	0.02128 min ⁻¹	92.6% (120 min)		73
MoS ₂ /Bi ₂ O ₃	Xe 250 W (λ > 420 nm),	HT, Sodium Molybdate, Thiourea)	20	50 mg (0.5g/L)	0.0138 min ⁻¹ , 0.276 min ⁻¹ g ⁻¹	79.3% (120 min)		81
a)C-ZnS/ZnMoO ₄ /MoS ₂ ; b)C-ZnS/MoS ₂	Xe 300 W (λ=320-780 nm)	HT, Ammonium Molybdate, Thiourea	15	15 mg (0.5g/L)	a) 0.016 min ⁻¹ , 1.067 min ⁻¹ g ⁻¹ b) 0.004 min ⁻¹ , 0.266 min ⁻¹ g ⁻¹			82
MoS ₂ /ZIF-8	Xe 300 W (λ > 420 nm)	ST Sodium Molybdate + Thioacetamide	20	20 mg (0.4g/L)	0.0049 min ⁻¹ , 0.245 min ⁻¹ g ⁻¹	75.6 % (180 min)		14
MoS ₂ /ZnSnO ₃		Exfoliated MoS ₂	30	25 mg (0.25g/L)	0.0226 min ⁻¹ , 0.904 min ⁻¹ g ⁻¹	80% (60 min)		83
MoS ₂ /Ag/g-C ₃ N ₄	Xe 300 W (λ > 420 nm)	HT, Ammonium Molybdate + Thiourea	20	10 mg (0.2g/L)	(PMS) 0.0837 min ⁻¹ , 8.37 min ⁻¹ g ⁻¹ (no PMS) 0.0507 min ⁻¹ , 5.07 min ⁻¹ g ⁻¹	98.9% (50 min, PMS)	45.2 % (no PMS) 69.5% (PMS)	99
MoS ₂ /CaTiO ₃	Xe 300 W	HT, Sodium Molybdate, Thiourea	10	50 mg (0.5g/L)	0.0505 min ⁻¹ , 1.01 min ⁻¹ g ⁻¹	71.7% (60 min)	70.6%,	107
MoS ₂ /g-C ₃ N ₄ /Bi ₂ O ₃ /Cl ₁₀	Xe 300 W (λ > 420 nm)	HT, Ammonium Molybdate, Thiourea	20	10 mg (0.2g/L)	0.0643 min ⁻¹ , 6.43 min ⁻¹ g ⁻¹	97.5% (50 min)		37
ZnS@MoS ₂	Hg 300 W (UV)	HT, Sodium Molybdate, Thiourea	20	100 mg (0.3g/L)		99.9% (60 min)		84
MoS ₂ /TiO ₂	Xe 300 W (λ > 420 nm)	HT, MoO ₃ , Thioacetic acid	20	1.0 mg (0.01 g/L)	0.0140 min ⁻¹ , 14 min ⁻¹ g ⁻¹	57% (in 60 min)		105
CdMoO ₄ /CdS/MoS ₂	Xe 300 W (λ > 420 nm)	HT, Ammonium Molybdate, Thiourea	40	50 mg (1g/L)	0.06446 min ⁻¹ , 1.3 min ⁻¹ g ⁻¹	99.69% (60 min)		85
BiOBr/MoS ₂ /GO	Xe 300 W (λ > 380 nm)	HT, Molybdate, Thiourea	20	25 mg (1g/L)	0.04277 min ⁻¹ , 1.71 min ⁻¹ g ⁻¹	98% (40 min)		86
MoS ₂ /Fe ₃ O ₄ /Cu ₂ O	Xe 300 W (UV filter)	HT, Ammonium Molybdate, Thioacetamide	20	10 mg (0.1g/L)		70% (90 min)		87
BiOI/MoS ₂		HT, Ammonium Molybdate, Thioacetamide	20	20 mg (0.307 g/L)	0.03514 min ⁻¹ , 1.76 min ⁻¹ g ⁻¹	91.5% (75 min)		88
MoS ₂ /B/Eu-g-C ₃ N ₄	Halogen 400W	HT, Ammonium Molybdate, Thiourea	20	20 mg(0.4g/L)	0.0873min ⁻¹ , 4.37 min ⁻¹ g ⁻¹	99% (50 min)		89
MoS ₂ /TiO ₂	W 300 W	HT, Sodium Molybdate + cysteine	10	10mg in 50ml (0.2g/L)	0.05 min ⁻¹ , 5 min ⁻¹ g ⁻¹	94% (60 min)		74
MoS ₂ /C ₃ N ₄	Xe 300 W (λ > 420 nm)	Exfoliated MoS ₂	5	0.5 mg (0.017 g/L)	0.053 min ⁻¹ , 106 min ⁻¹ g ⁻¹	91.7 % (60 min)		106
MoS ₂ /Zeol/CeO ₂	Xe 300 W	HT, Ammonium Molybdate, Cysteine	10	10 mg (0.2g/L)	0.022 min ⁻¹ , 2.2 min ⁻¹ g ⁻¹	98.32% (150 min)		75
MoS ₂ /c- mica	Xe 300W 150 mW/cm ²	HT, Sodium Molybdate, Thioacetamide	20	20 mg (0.2g/L)	0.063 min ⁻¹ , 3.15 min ⁻¹ g ⁻¹			90
MoS ₂ /ZnWO ₄	100 W solar simulator (λ >	HT, Ammonium Molybdate +Thiourea	10	15 mg (0.2g/L)	0.0334 min ⁻¹ , 2.23 min ⁻¹ g ⁻¹	97.40% (105 min)		76

	400 nm							
MoS ₂ /B-rGO	Xe 300 W	HT, Sodium Molybdate, Thiocarbamide	20	20 mg (0.4g/L)		85.3% (90 min)		91
Cu ₂ O/MoS ₂ /rGO	Halogen 150W	HT, Sodium Molybdate, Thiourea)	20	30 mg (0.3g/L)	0.184 min ⁻¹ 6.13min ⁻¹ g ⁻¹ (sonophotocat) 0.03 min ⁻¹ 1 min ⁻¹ g ⁻¹ (photocat)	100% (10 min) (sonophotocat) 95% (60 min) (photocat)		100
Fe ₂ O ₃ /MoS ₂ /SDS	NIR 808 nm 0.7 W/cm ²	HT, Sodium Molybdate + Thioacetamide	25	12 mg 0.24g/L)	0.016 min ⁻¹ 1.33 min ⁻¹ g ⁻¹	92.3% (120 min)		117
BiVO ₄ / MoS ₂		HT, Ammonium molybdate + thiourea	40	15 mg (0.3g/L)	0.0337 min ⁻¹ 2.25 min ⁻¹ g ⁻¹	97.46% (90 min)		39
Pt-MoS ₂ /BiVO ₄	Xe 250W	HT, Ammonium molybdate, Thiourea	20	0.1g, (1g/L)	0.0137 min ⁻¹ 0.137 min ⁻¹ g ⁻¹	62.5% (80 min)		92
TiO ₂ /MoS ₂ /BiVO ₄	Xe 300 W (λ > 420 nm)	HT, Sodium Molybdate, Thiourea	20	40 mg (1g/L)		90.3% (90 min)	56.3%	108
MoS ₂ /TiO ₂ /G	Tungsten (12 W cm ⁻²)	HT, Sodium Molybdate, Cysteine	10	10 mg, 0.01g/L	0.048 min ⁻¹ 4.8 min ⁻¹ g ⁻¹	94.5 % (60min)	66.2%	18
MoS ₂ /Ag ₃ PO ₄	Xe 235 W	HT, Sodium Molybdate, Thiourea	10	50 mg (0.5 g/L)	0.033 min ⁻¹ 0.66 min ⁻¹ g ⁻¹	93% (60 min)		49
MnFe ₂ O ₄ /MoS ₂	Xe 300 W (λ > 420 nm) 398.75 mW/cm ²	ST, Ammonium Molybdate, Thiourea	10	20 mg (0.2 g/L)		76.4% (60 min)		77
MoS ₂ /Bi ₂ WO ₆	100 W solar simulator	HT, Ammonium Molybdate, Thiourea	10	15 mg (0.3g/L)	0.0309 min ⁻¹ 2.06 min ⁻¹ g ⁻¹	96.30% (90 min)		78
Bi-MOF/BiOCl/MoS ₂	Xe 300 W (λ > 420 nm)	HT, Sodium Molybdate, Thiourea	10	10 mg (0.2g/L)	0.104 min ⁻¹ 10.4 min ⁻¹ g ⁻¹	90% (20 min)		97
NH ₂ -MIL-88B (Fe)/MoS ₂	Xe 300 W (λ > 400 nm)	HT, Ammonium Molybdate, Thiourea	20	50 mg (0.5g/L)	0.056 min ⁻¹ 1.12 min ⁻¹ g ⁻¹	96.44% (60 min)	>72%	93
NiSe ₂ /MoS ₂	Xe 300 W	HT, Ammonium Molybdate, Thiourea	20	30 mg (0.6 g/L)	0.01272 min ⁻¹ 0.424 min ⁻¹ g ⁻¹	80.6% (120 min)	58.1%	109
MoS ₂ /In ₂ S ₃ /Bi ₂ S ₃	Xe 300 W (λ > 420 nm)	HT, Sodium Molybdate, Thiourea	10	30 mg (1g/L)	0.05049 min ⁻¹ 1.683 min ⁻¹ g ⁻¹	99.6% (90 min)	93%	79
MoS ₂ /TiO ₂	Halide 400 W	Exfoliated MoS ₂	10	25mg (0.25g/L)	0.0276 min ⁻¹ 0.276 min ⁻¹ g ⁻¹			80
CdS/MoS ₂ / WS ₂	Xe 150W (λ > 420 nm)	HT, Ammonium Molybdate, Thiourea	20	0.01 g (0.1 g/L)	0.055 min ⁻¹ 5.5 min ⁻¹ g ⁻¹	97.2% (60 min)		30
MoS ₂ /C ₃ N ₄ /ZIF8	Xe 500 W (λ > 420 nm)	HT, Sodium Molybdate, Thioacetamide	OTC 10	10 mg (0.166 g/L)		97% (5 min) (photophenton)	28.8%	101
BiOBr/MoS ₂	LED 5 W 160 mW cm ⁻²	Hydrothermal, MoO ₃ , KSCN	10	20mg, (0.4 g/L)	0.0211 min ⁻¹ 1.055 min ⁻¹ g ⁻¹	95.9% (90 min)	62.9% (135 min)	110
Ag ₃ PO ₄ /MoS ₂		HT, Sodium Molybdate, Thiourea	10	20 mg (0.2g/L)	1.04 min ⁻¹ 52 min ⁻¹ g ⁻¹	98.9% (10 min)	46.3% (150 min)	28
MoS ₂ /SnWO ₄	100 W (λ > 400 nm)	HT, Ammonium Molybdate, Thiourea	10	15 mg (0.3g/L)	0.0372 min ⁻¹ 2.48 min ⁻¹ g ⁻¹	96.47% (80 min)		65
MoS ₂ /G Aerogels	Hg 250 W (λ > 420 nm)	HT, Sodium Molybdate, Cysteine	5	50 mg (0.5 g/L)		91% (120 min)	24%	66
ZVI Fe/MoS ₂	Xe 300 W (λ > 420 nm)	HT, Ammonium Molybdate, Thiourea	30	10 mg (0.167 g/L)	0.033 min ⁻¹ 3.3 min ⁻¹ g ⁻¹	97% (45 min)		32
MoS ₂ /TiO ₂	Xe 500 W (λ > 420 nm)	HT, Sodium Molybdate, Thiourea	35	30 mg (0.6g/L)	0.0236 min ⁻¹ 1.2 min ⁻¹ g ⁻¹	95.4% (120 min)		31
MoS ₂ /TiO ₂	Xe 300 W (λ > 420 nm)	HT, MoO ₃ , Thioacetamide	20	30 mg (0.3g/L)	0.007 min ⁻¹ 0.23 min ⁻¹ g ⁻¹			19
CNTs/CdS/MoS ₂		HT, Sodium Molybdate, Thiourea	10	0.1g (1g/L)		96.7% (100 min)		67
MoS ₂ QDs /C ₃ N ₄	Xe 300 W (λ > 400 nm)	HT, Sodium Molybdate, Thiourea	20	20 mg	0.145 min ⁻¹ 4.83 min ⁻¹ g ⁻¹	96% (30 min)	88.8%	98
MoS ₂ /BiVO ₄	Xe 300 W (λ > 420 nm)	HT, Sodium Molybdate, Thiourea	5	50 mg (0.5 g/L)	0.0215 min ⁻¹ 0.43 min ⁻¹ g ⁻¹	93.7% (90 min)		68
PCN-224@MoS ₂	Xe 500 W (λ > 420 nm), 100 mW/cm ²	HT, Sodium Molybdate, Thiourea	20	8 mg (0.2 g/L)	0.0525 min ⁻¹ 6.56 min ⁻¹ g ⁻¹	96.41 % (60 min)		29
MoS ₂ /MXene	Xe, 0.16 mW/m ²	HT, Sodium Molybdate, Thiourea	OTC 50	100 mg (0.5 g/L)	0.0304 min ⁻¹ 0.304 min ⁻¹ g ⁻¹	89% (60 min)	83%	94
MoS ₂ /CuBi ₂ O ₄	Xe 100W	HT, Ammonium Molybdate,	5	30 mg (0.6g/L)	0.00412 min ⁻¹ 0.14 min ⁻¹ g ⁻¹	93% (180 min)		69

		Thioacetamide							
Cu ₂ WS ₄ /MoS ₂	Xe 500 W ($\lambda > 420$ nm)	HT, Sodium Molybdate, Thioacetamide	100	40 mg (0.4g/L)	0.0312 min ⁻¹ 0.78 min ⁻¹ g ⁻¹	93.3% (90 min)	72.1% (90 min)	95	
Ag/CAU-17@MoS ₂	Xe 300 W ($\lambda > 420$ nm)	HT, Sodium Molybdate, Thiourea	10	30 mg (1g/L)	0.02473 min ⁻¹ 0.824 min ⁻¹ g ⁻¹	91.6 % (120 min)	90 %	70	
Ag ₃ PO ₄ /Fe ₃ O ₄ /MoS ₂	Xe 500 W ($\lambda > 420$ nm), 72.4 mW/cm ²	HT, Sodium Molybdate, Thiourea	10	20 mg (0.2 g/L)	0.157 min ⁻¹ 7.9 min ⁻¹ g ⁻¹	99 % (5 min)	44.2 % (60 min)	20	
MnFe ₂ O ₄ /MoS ₂		HT, Ammonium Molybdate, Thiourea	10	(0.1 g/L)	0.150 min ⁻¹ (PMS)	92.9 % (30 min)	70.5%	102	
MoS ₂ /G Aerogel	Hg 250 W ($\lambda > 420$ nm)	HT Sodium Molybdate, Cysteine	5	50 mg (0.5 g/L)	0.0211 min ⁻¹ 0.42 min ⁻¹ g ⁻¹	97 % (120 min)	67%	71	
MoS ₂ /CdS	Xe 300 W ($\lambda > 420$ nm)	HT, MoO ₃ , Thioacetamide	50	50 mg (0.5 g/L)	0.0235 min ⁻¹ 0.47 min ⁻¹ g ⁻¹	70.8%		21	
MoS ₂ /BN	Xe 350 W ($\lambda > 420$ nm)	HT, Sodium Molybdate, Thiourea	10	10 mg (0.1g/L)	0.0438 min ⁻¹ 4.38 min ⁻¹ g ⁻¹			72	
MoS ₂ /MXene		HT, Sodium Molybdate, sodium diethyldithiocarbamate	10	20 mg (0.4 g/L)	0.1447 min ⁻¹ 7.24 min ⁻¹ g ⁻¹ (PDS)	100% (60 min)	75.30%	103	
MoS ₂ / α -Fe ₂ O ₃	UV 15 W 0.23 mW/cm ²	HT, Ammonium Molybdate, Thiourea	20	2 mg (0.2g/L)		60 % (180 min)		96	
MoS ₂ /g-C ₃ N ₄ /AgI	Xe 300 W ($\lambda > 400$ nm), 70 mW/cm ²	ST, Ammonium tetrathiomolybdate	10	30 mg (0.5g/L)	0.043 min ⁻¹ 1.43 min ⁻¹ g ⁻¹	82.8% (50 min)	53%	111	
TiO ₂ /n-C/MoS ₂ /Ag	Xe 300 W	HT, Ammonium Molybdate, Thiourea	10	Membrane 3 x3 cm ²	0.156 min ⁻¹ (PMS) 0.039 min ⁻¹ (no PMS)	97.4 % (20 min)	57.5%	104	
SiO ₂ /MoS ₂ /Cu ₂ O	Warm LED, ($\lambda > 420$ nm, max. 600 nm) (52x10 ⁻³ W cm ²)	ST, Ammonium tetrathiomolybdate	5-10	Supported 2x2 cm ² , 73 μ g (0.004g/L)	0.013 min ⁻¹ 178 min ⁻¹ g ⁻¹ (pH=6), 0.014 min ⁻¹ 192 min ⁻¹ g ⁻¹ (pH=8)	90 % (pH=6) 92 % (pH=8) (180 min)	74.6 % (pH=6) 86.2 % (pH=8) (180 min.)	This work	

*Refer to the main text for the references in the table

4. Photocatalytic performance of Silica/Cu₂O and Silica support

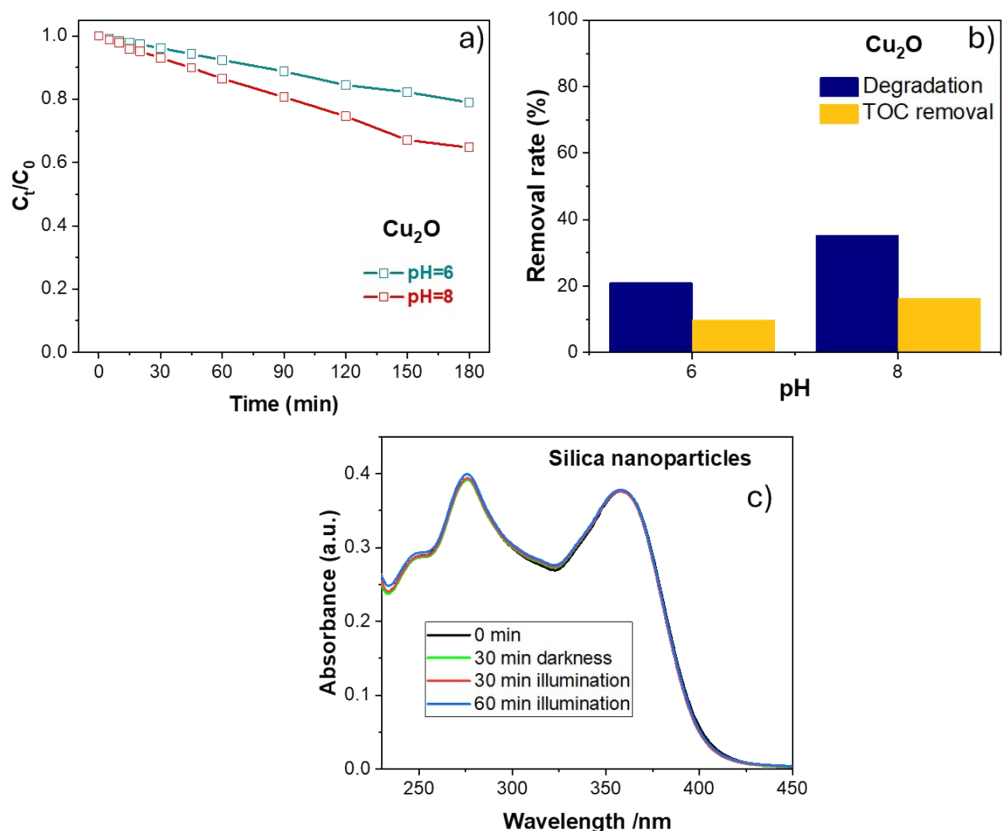


Figure S3. a) Variation of the TC concentration versus time at different pHs for the system Silica/Cu₂O. b) Degradation and TOC removal percentage for Silica/Cu₂O. c) Absorbance of TC in the dark and as function of illumination time for the supported silica nanoparticles.

5. Electron paramagnetic resonance (EPR) measurements

Electron paramagnetic resonance measurements confirmed the generation of hydroxyl radicals in all tested systems: silica/Cu₂O, silica/MoS₂, and silica/MoS₂/Cu₂O. However, each system exhibited complex spectral features arising from secondary interactions between DMPO, the radical adducts and the photocatalyst surface.

In the Silica/Cu₂O system, a characteristic signal corresponding to the DMPO–OH adduct was observed even under ambient light. Additionally, a second spin adduct was detected, likely resulting from interactions between DMPO and copper species at or near the photocatalyst surface (Figure S4). This secondary interaction can interfere with the ability of DMPO to react with other ROS, promoting other reaction pathways, as described in the literature.

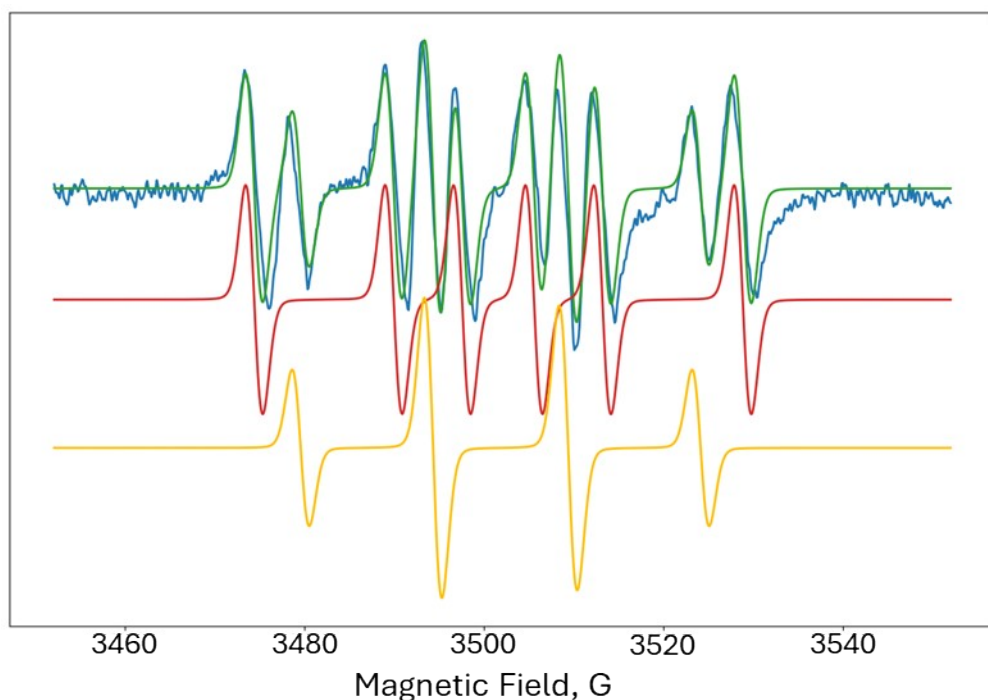


Figure S4. EPR spectrum of Silica/Cu₂O/DMPO system under ambient light. Experimental data (blue line) together with the simulated response (green line). The spectrum is modelled as a mixture of two paramagnetic species (red and dark yellow curves). The lower signal (dark yellow line) corresponds to the DMPO-OH adduct ($A_N = 15.1$ mT, $A_H = 14.6$ mT), contributing approximately 40%. The red simulated spectrum, $A_N = 15.7$ mT, $A_H = 23.3$ mT is likely associated with secondary reaction pathways.

For the Silica/MoS₂ system, the EPR signal also contained multiple components (Figure S5). One of them, identified as the DMPO-OH adduct (dark yellow curve), confirmed the presence of hydroxyl radicals. Upon increasing light intensity, this signal became more pronounced, while secondary components diminished, indicating efficient and light-dependent generation of hydroxyl radicals (Figure S6).

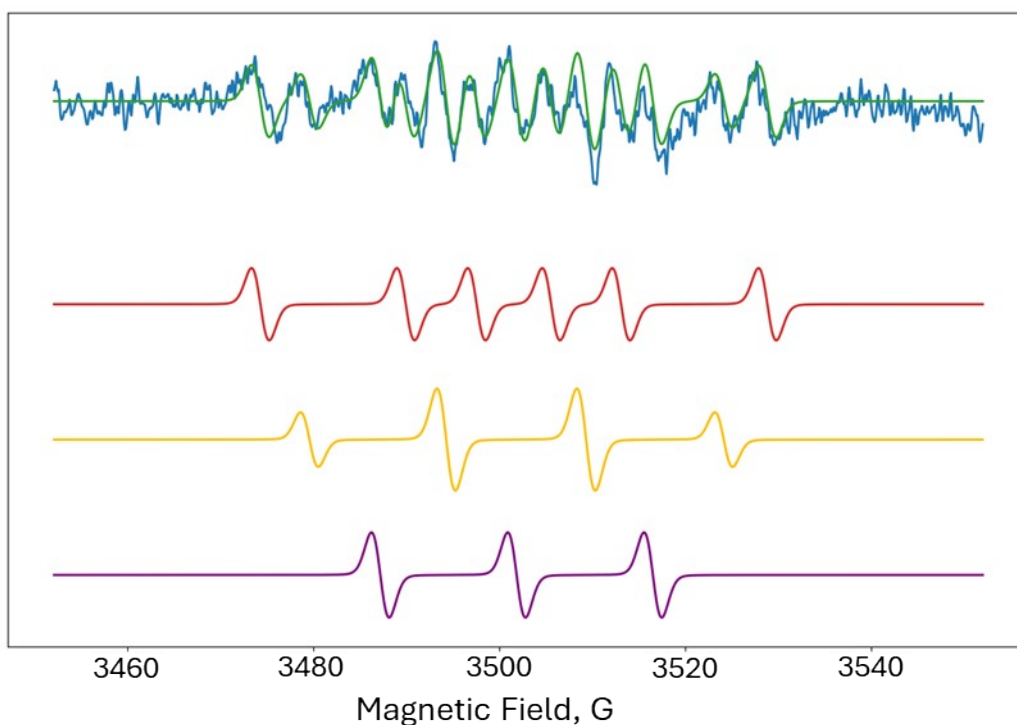


Figure S5. EPR spectrum of Silica/MoS₂/DMPO system under ambient light. Experimental data (blue line) and simulated response (green line), composed of three components: DMPO–OH (dark yellow), and two additional species, red ($A_N = 15.1$ mT, $A_H = 14.6$ mT) and violet ($A_N = 14.7$ mT) curves.

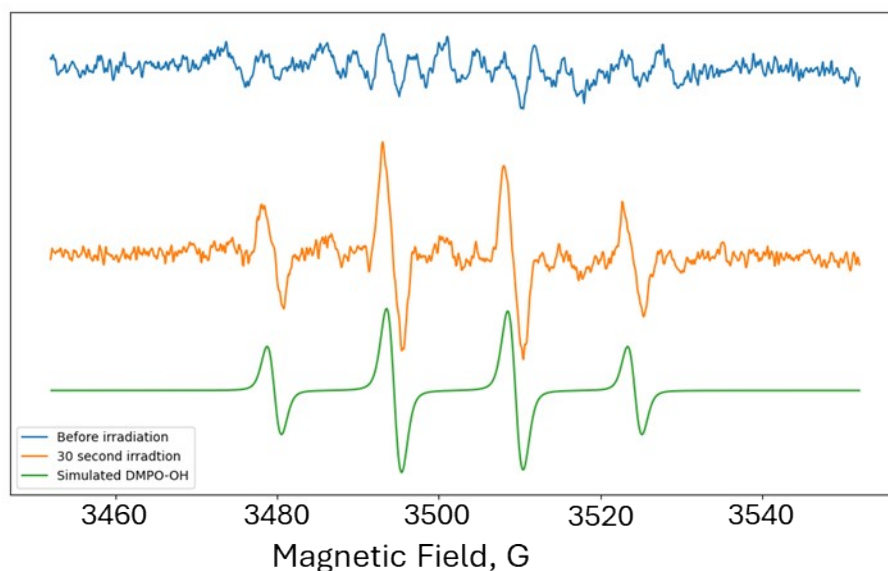


Figure S6. EPR spectra of Silica/MoS₂/DMPO system under ambient light (blue line) and under white light irradiation (orange line). The DMPO–OH signal significantly increases with illumination. The simulated DMPO–OH response is shown in green.

For the Silica/MoS₂/Cu₂O system, the EPR response under ambient light was more intense than in the Silica/MoS₂ sample (Figure S7), with a clear DMPO–OH component. However, upon irradiation, the overall signal increase was dominated by an adduct with six-line pattern likely related to DMPO–metal interactions, rather than an amplified

hydroxyl generation (Figure S8). This behavior highlights the interference caused by copper species, which may quench or mask the formation of other ROS and complicate spectral analysis.

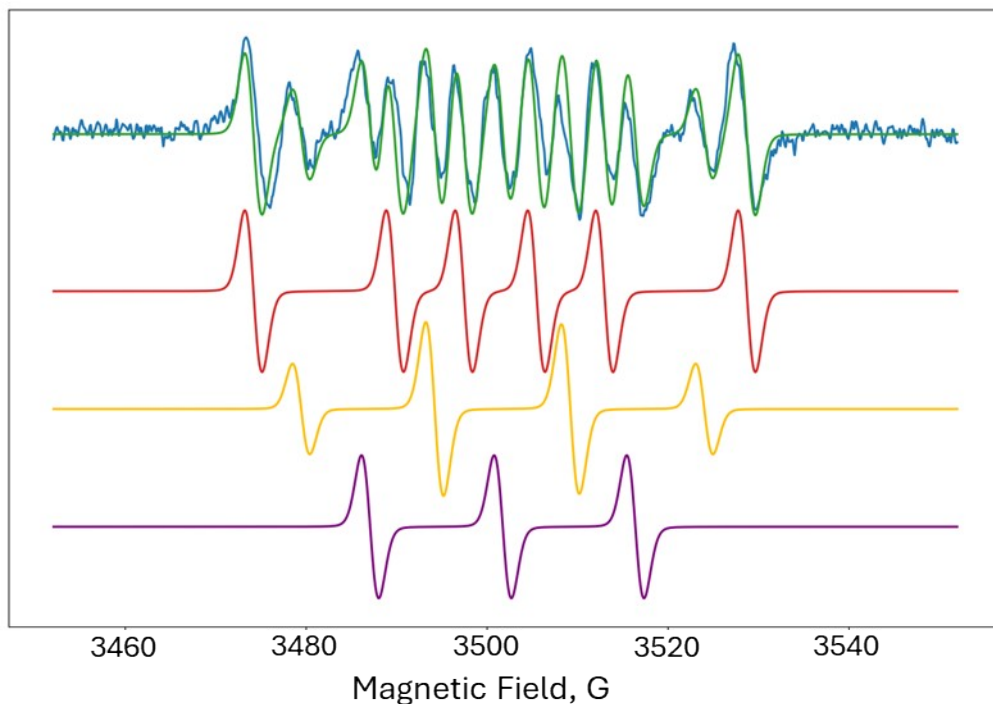


Figure S7. EPR spectrum of Silica/MoS₂/Cu₂O/DMPO system under ambient light. Experimental data (blue line) and simulated fit (green line), composed of three species including the DMPO–OH adduct (dark yellow curve).

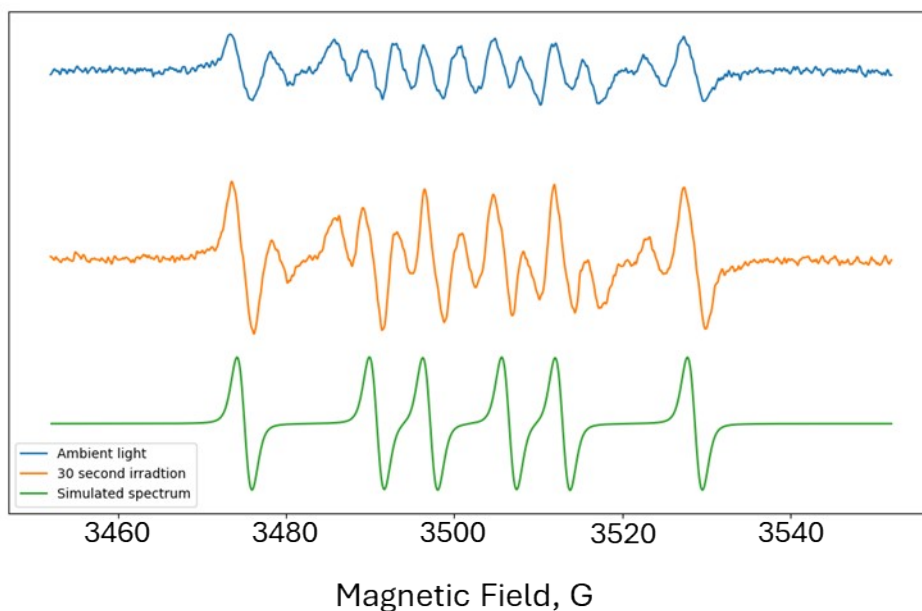


Figure S8. EPR spectra of Silica/MoS₂/Cu₂O/DMPO system under ambient (blue line) and higher light intensity (orange line). The increase in spectral intensity upon irradiation is primarily due to increase in the six-line signal attributed to secondary reaction pathways. The simulated spectrum obtained from the fit of this signal is shown in green.

6. Spectroscopic characterization of the photocatalyst after photocatalytic degradation cycles

Spectroscopic analyses (XPS and Raman) were employed to assess the impact of photocatalyst reusability. Raman spectroscopy showed minimal variation, while XPS revealed a slight increase in the 2H-MoS₂ phase after extended use. Importantly, the Cu₂O component consistently maintained its +1 oxidation state throughout the tests.

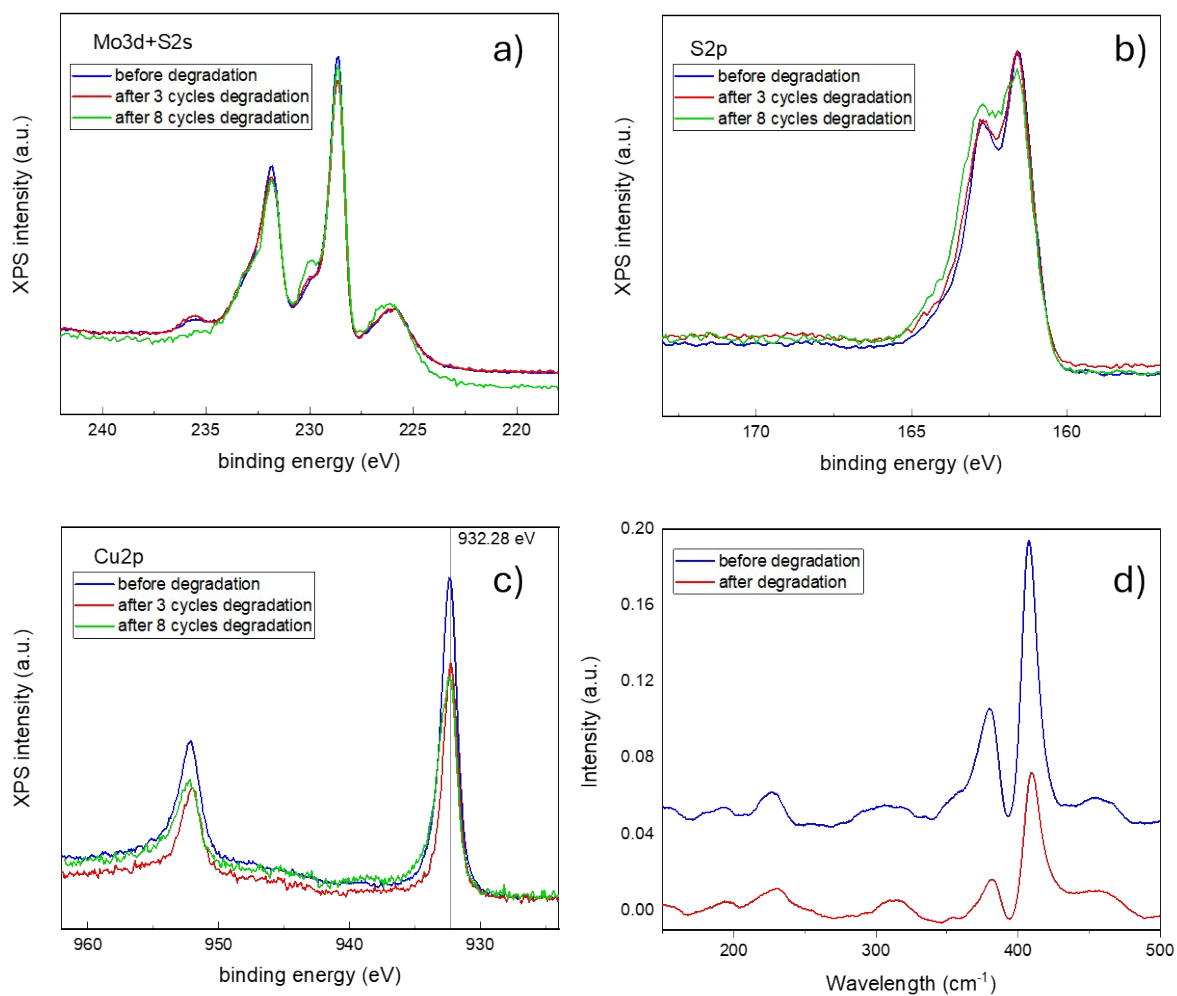


Figure S9. (a–c) XPS spectra of the ST MoS₂/Cu₂O system before and after multiple degradation cycles. (d) Raman spectra of the system before and after multiple degradation cycles.

7. Photocatalytic Degradation in more complex matrices

Table S2. Degradation of multi-pollutants in MilliQ water

MULTI-POLLUTANT MilliQ-water	[TC]= 10 ppm [ANATOXIN-a]= 10 ppm			
pH	6.0	8.0	6.0	8.0
Time / min	TOC	TOC	MINERALIZATION %	MINERALIZATION %
0	21.231	21.231	0.00	0.00
180	6.964	5.499	67.20	74.10
240	3.97	3.121	81.30	85.30

Table S3. Degradation of multi-pollutants in MilliQ water

MULTI-POLLUTANT Tap water	[TC]= 10 ppm [ANATOXIN-A]= 10 ppm			
pH	6.0	8.0	6.0	8.0
Time / min	TOC	TOC	MINERALIZATION %	MINERALIZATION %
0	26.44	26.44	0.00	0.00
180	4.35	3.34	83.54	87.38
240	1.99	1.04	92.49	96.08

Table S4. Composition of the tap water

Organic Carbon Content	4.991	
Alkalinity (CaCO ₃)	200.5	mg L ⁻¹
Bicarbonate (HCO ₃ ⁻)	156	mg L ⁻¹
Calcium	72.3	mg L ⁻¹
Chloride	86.5	mg L ⁻¹
Nitrate	5.36	mg L ⁻¹
Sulphate	79.4	mg L ⁻¹
Sodium	92.1	mg L ⁻¹
Potassium	11.3	mg L ⁻¹

8. Band-gap and band edges estimation

The band gaps of the system were determined using UV–Vis diffuse reflectance spectroscopy (DRS) in combination with Kubelka-Munk analysis (Fig.S10). Due to the multilayer nature of MoS₂, the indirect band gap formalism was

applied, resulting in a band gap value of approximately 1.97 eV. This value is slightly higher than typical for the 2H-phase of MoS₂, potentially due to contributions from molybdenum oxide, as indicated by XPS analysis. Furthermore, XPS suggested that the 1T' phase of MoS₂ may behave as a very low band gap semiconductor, with almost metallic character. However, its precise determination was beyond the capabilities of the equipment, as wavelengths greater than 1000 nm would be required. For Cu₂O, the band gap was measured at 1.89 eV, consistent with values expected for this material [1].

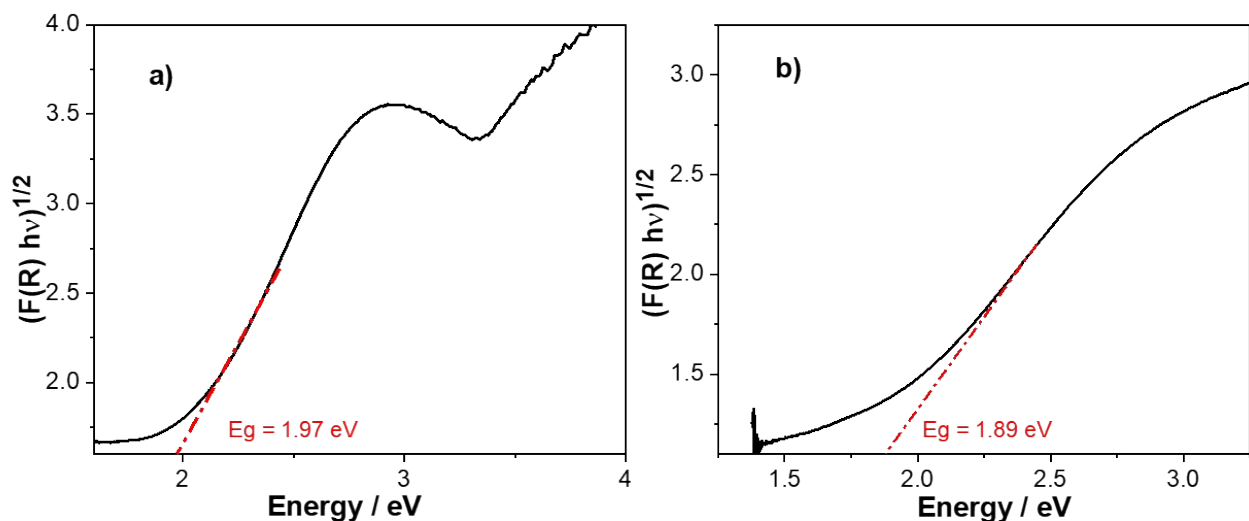


Figure S10. Band gap estimation of MoS₂ (a) and Cu₂O (b) respectively.

Instead of relying on theoretical calculations based on the absolute electronegativity of the materials to determine the valence band (VB) and conduction band (CB) edge potentials of MoS₂ and Cu₂O, as is common in most reported studies, we used photoemission spectroscopy for a more accurate assessment. Precisely determining electron transfer pathways remains particularly challenging due to the inherent complex multiphase characteristic of these materials.

Specifically, we determined the valence band maximum (VBM) positions of 2H-MoS₂ and isolated 1T'-MoS₂ separately by measuring firstly their VBMs relative to the Fermi level. For capturing the unstable 1T' phase, measurements were conducted immediately after synthesis to prevent 2H phase transformation or oxidation from ambient oxygen. The stable 2H phase was characterized using a bulk 2H-MoS₂ natural crystal. Figure S11a shows the XPS valence band of MoS₂ 1T' referenced to the analyzer Fermi level (0 eV binding energy), with the extrapolations of the leading edge (discontinuous grey line from the convergence of all the curves) indicating the valence band maximum. In the case of 2H MoS₂, the valence band maximum with respect to the Fermi level is shown at the inset of Fig. 4 a of the main text. The ionization potentials (IP) were then calculated using the secondary electron cutoff (SECO) (Fig. S11b) and the corresponding VBM values according to the relation:

$$IP = hv - (SECO - VBM),$$

with $hv = 21.22\text{eV}$ (UPS). In the case of Cu₂O, the VBM relative to the Fermi level was measured to be approximately 0.4 eV, as shown in Figure S11a. This value was captured from the solvothermal MoS₂/Cu₂O sample (second extrapolated dashed line from the red line). The work function of Cu₂O, 4.5 eV, was taken from Reference 1.

Figure S11c illustrates the band diagrams of the individual components (2H-MoS₂, 1T'-MoS₂, Cu₂O) as well as the combined systems: the solvothermal MoS₂ (mixture of 2H/1T' MoS₂) and the solvothermal MoS₂/Cu₂O composite, referred to the Fermi level. Note that in Fig. 10 in the main text, the energies are referred to the normal hydrogen

electrode (NHE) scale, by subtracting 4.44 eV, assuming a common vacuum level. Here, with the energy levels referred to the Fermi level, a maximum vacuum level shift, i.e., potential barrier, of 0.4 eV is observed, indicating that band bending at the interfaces is small and unlikely to introduce substantial band bending barriers to charge transfer processes.

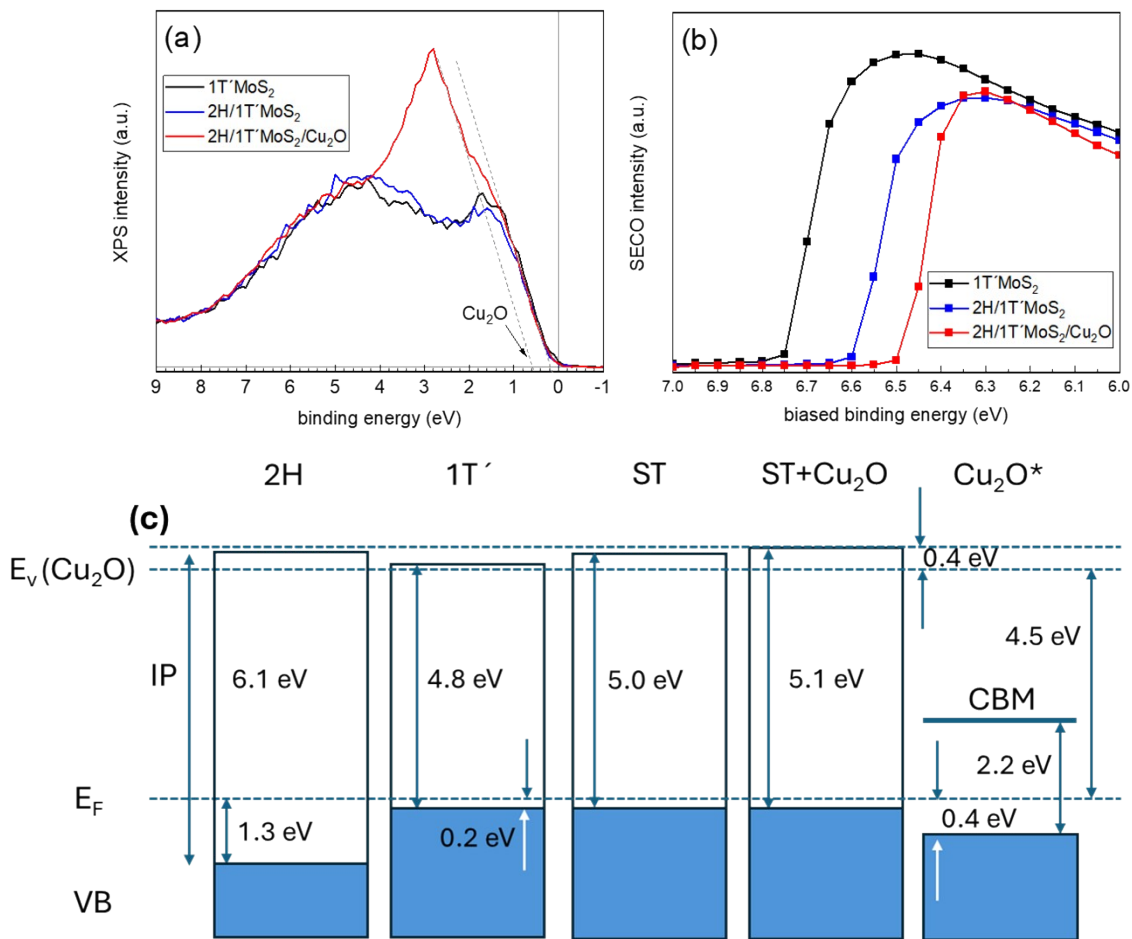


Figure S11. (a) XPS valence band of samples 1T' MoS₂, 2H/1T' MoS₂ and 2H/1T' MoS₂ + Cu₂O referred to the analyzer Fermi level (0 eV binding energy) and showing the extrapolations of the leading edges (discontinuous grey lines). (b) Secondary electrons cut-off (SECO) upon polarization of the sample at -10 V (see Materials and Methods for details) of the same samples. The red curve in (a) evidences the contribution of Cu states to the valence band, centered at about 3 eV binding energy, which allows the evaluation of the band offset between the 1T' MoS₂ phase and Cu₂O with both extrapolations, giving an approximated value of 0.4 eV. The SECO onsets provide a direct measurement of the band bending barriers among the different samples with a maximum value of 0.15 eV between the 1T' and 2H/1T' MoS₂+Cu₂O samples. (c) Diagram showing the valence band maximum relative to the vacuum level, denoted by the ionization potential, for 1T' MoS₂, 2H MoS₂, ST MoS₂ (which contains the mixed phases) and ST MoS₂/Cu₂O. The upper dashed lines correspond to the Cu₂O vacuum level (as indicated) and that of the ST MoS₂/Cu₂O.

Photoemission spectra in presence of light

XPS measurements were performed under dark and light conditions. However, no substantial changes were observed in such measurements as depicted in Fig S12 a and b.

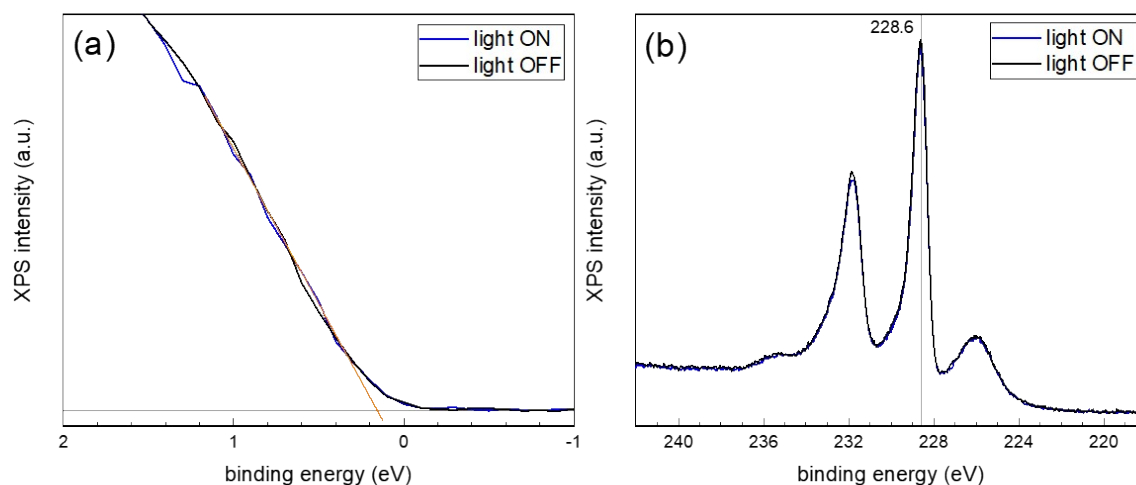


Figure S12. XPS spectra of a ST MoS₂+Cu₂O sample showing (a) the valence band edge and (b) the Mo3d-S2s lines acquired under dark conditions (light off) and under illumination (light on), respectively, using an external Thorlabs MWWHLP1 white light LED (3000 K) with a focusing lens. The valence band maximum (VBM), located at about 0.15 eV below the Fermi level, is obtained by a linear extrapolation (orange line) of the leading edges in the valence band spectra and the binding energy of the Mo3d_{5/2} feature (228.6 eV) is indicated. The results shown here evidence that illumination with white light does not induce any energy shift in the spectra, which are essentially identical. Same results have been obtained for the S2p lines (not shown).

9. Bioassays: In vitro experiments and additional ROS characterization

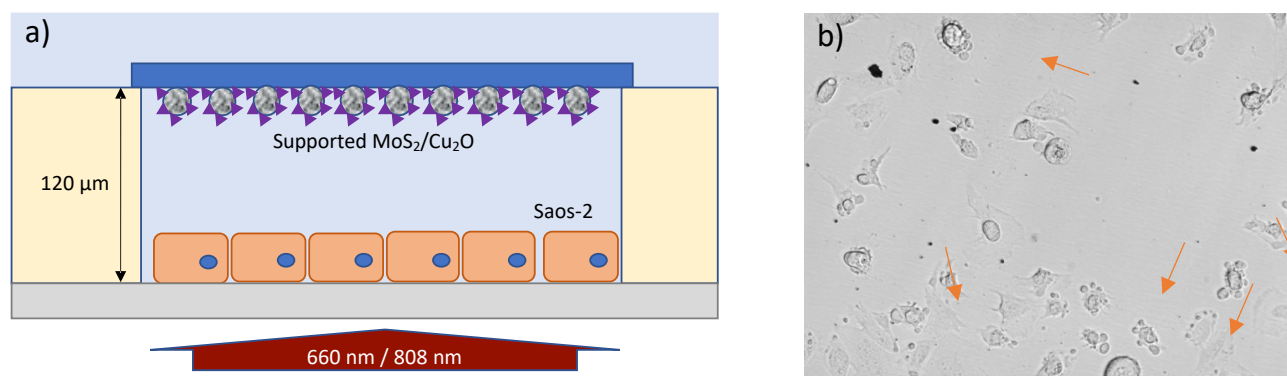


Figure S13. (a) Schematic of the in vitro assay with Saos-2 cells and the supported MoS₂/Cu₂O nanoflakes at a separation distance of 120 μ m from the cells. (b) Representative bright field image showing cells undergoing apoptosis (arrows).

The individual photodynamic effects of silica/MoS₂ and silica/Cu₂O on cell viability are shown in Fig. S14 after illumination with the NIR laser for 30 minutes at 100 mW/cm². Minimal cell death was observed, indicating low photodynamic activity for the individual components.

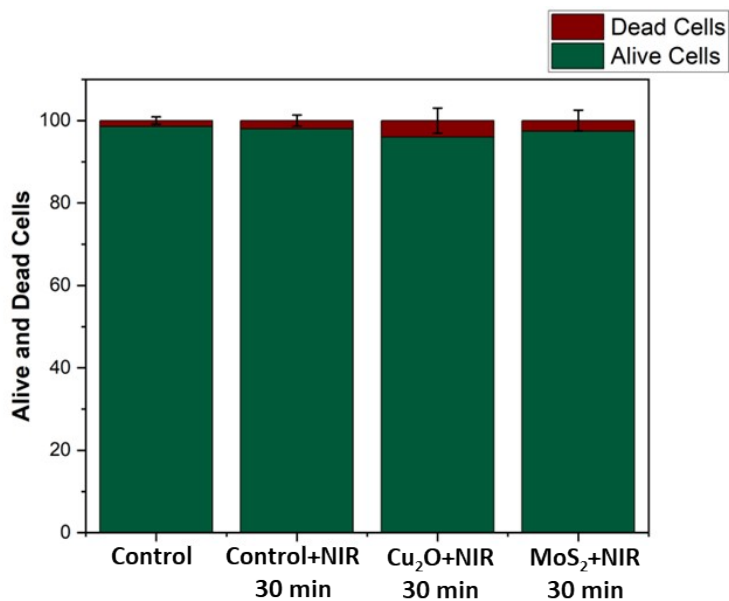


Figure S14. Cell viability after treatment with silica/MoS₂ and silica/Cu₂O nanomaterials following NIR laser illumination (30 min, 100 mW/cm²).

Intracellular ROS generation was also assessed using the DCF-DA fluorescence method. DCF-DA is a cell-permeable, non-fluorescent probe that diffuses into cells and is hydrolyzed by intracellular esterases to form the non-fluorescent compound DCFH. This compound is selectively oxidized by intracellular ROS, particularly those generated through peroxidase and iron-catalyzed reactions, to yield the highly fluorescent DCF. Cells were incubated with 10–20 μM DCF-DA in serum-free medium at 37°C for 30 minutes in the dark. After staining, cells were washed with PBS to remove excess dye. To validate the assay and serve as a positive control, cells were treated with 100 μM hydrogen peroxide (H₂O₂), a known inducer of intracellular oxidative stress. Fluorescence was detected using a fluorescence microscope (excitation at 488 nm and emission at 525 nm), with untreated cells included as negative controls to establish baseline ROS levels. Strong fluorescence was observed in H₂O₂-treated cells, confirming ROS generation, while untreated and MoS₂/Cu₂O-treated cells exhibited minimal fluorescence, indicating low intracellular ROS levels under the tested conditions.

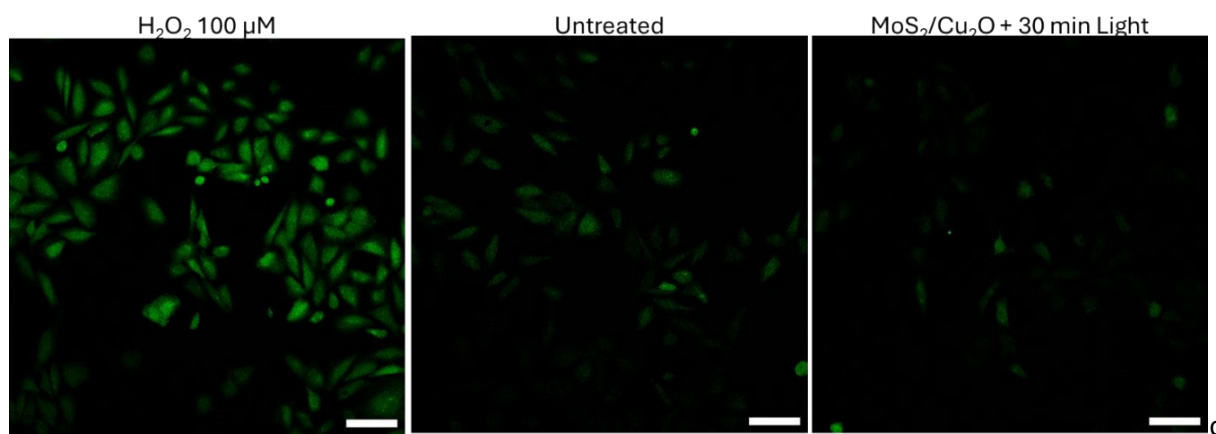


Figure S15. Fluorescence microscopy images showing intracellular ROS levels in cells treated with hydrogen peroxide (H₂O₂, 100 μM) as positive control, untreated controls, and in presence of MoS₂/Cu₂O exposed to light for 30 minutes. Scale bar 100 μm.

References

- 1 Y. Luo, L. Niu, Y. Wang, P. Wen, Y. Gong, C. Li and S. Xu, *Appl. Surf. Sci.*, 2023, **607**, 155095.